High Temperature. Vol. 44, No. 4, 2006, pp. 497–506. Translated from Teplofizika Vysokikh Temperatur, Vol. 44, No. 4, 2006, pp. 503–511.

PLASMA INVESTIGATIONS

The Spatial Structure of a Current Layer in an MGD Channel

E. N. Vasil'ev and D. A. Nesterov

Institute of Computational Modeling, Siberian Division, Russian Academy of Sciences, Krasnoyarsk, 660036 Russia

Received May 16, 2005

Abstract—The numerical solution of an unsteady-state three-dimensional set of equations of radiation gas dynamics is used to investigate the process of formation of a current layer in an MGD channel. It is found that the structure of current layer and the integral characteristics of interaction at low and high pressures are different because of the different patterns of radiation (volume and surface, respectively). The processes of flow past the discharge region and the division of this region into several current-conducting channels because of the development of Rayleigh–Taylor instability result in a decrease in the efficiency of MGD interaction.

INTRODUCTION

One of the main factors defining the efficiency of magnetogasdynamic (MGD) interaction is the electrical conductivity of the medium. In MGD flows with a self-sustaining current layer (T-layer), the electrical conductivity is supported by the thermal ionization of gas in the local plasma zone of flow, which interacts with the external magnetic field and nonconducting gas. The numerical simulation of the process in a two-dimensional formulation with a constant value of the load factor revealed that a mode of nonconducting gas flow past the current layer sets in under conditions of MGD interaction; in so doing, a vortex wake is formed downstream [1]. In addition, Rayleigh–Taylor instability (RTI) may develop on the upstream boundary of the T-layer where media of different densities are in contact and the force of gasdynamic pressure is effective; this instability leads to the division of the discharge region into two or several current-conducting channels. The characteristics of the MGD process depend on the current layer structure (the size and the distribution of electrical conductivity); therefore, its variation because of the vortex separation and division of the discharge region leads to significant fluctuations of the values of characteristics in time. The inclusion of the factors of flow and development of RTI in a two-dimensional model produced a significant difference in the integral characteristics of the process compared to those obtained in a one-dimensional approximation. More complete information about the pattern of flow in an MGD channel may be obtained as a result of computational simulation in a three-dimensional formulation. It is the objective of this study to determine the spatial form of current layer and the effect of this form on the structure of flow and integral characteristics of the process of MGD interaction for different values of pressure in the channel.

FORMULATION OF THE PROBLEM AND METHOD OF SOLUTION

We will treat the flow of a nonviscous radiating gas in a channel of constant square cross section with solid electrodes closed on an external ohmic load (Fig. 1). The nonconducting flow includes a local plasma region interacting with a transverse magnetic field. In so doing, induced electric current flows in the

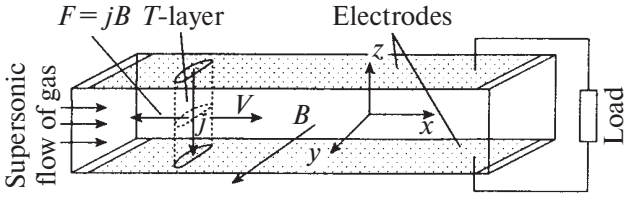

Fig. 1. Diagrammatic view of the process in the channel of an MGD generator with a T-layer.

0018-151X/06/4404-0497

"current layer–electrodes–load" circuit. The computational model of the process is based on the solution of equations of gas dynamics, Maxwell equations, and equation of radiative transfer.

Set of Equations

The motion of gas is described using a set of Euler equations

$$\frac{\partial \mathbf{U}}{\partial t} + \frac{\partial \mathbf{E}}{\partial x} + \frac{\partial \mathbf{F}}{\partial y} + \frac{\partial \mathbf{G}}{\partial z} = \mathbf{S}, \qquad (1)$$

$$\mathbf{U} = \begin{bmatrix} \rho \\ \rho u \\ \rho v \\ \rho w \\ E_t \end{bmatrix}, \quad \mathbf{E} = \begin{bmatrix} \rho u \\ \rho u^2 + p \\ \rho uv \\ \rho uw \\ (E_t + p)u + q_x \end{bmatrix},$$

$$\mathbf{F} = \begin{bmatrix} \rho v \\ \rho vu \\ \rho v^2 + p \\ \rho vw \\ (E_t + p)v + q_y \end{bmatrix}, \quad \mathbf{G} = \begin{bmatrix} \rho w \\ \rho wu \\ \rho wv \\ \rho w^2 + p \\ (E_t + p)w + q_z \end{bmatrix}, \qquad (2)$$

$$\mathbf{S} = \begin{bmatrix} 0 \\ f_x \\ f_y \\ f_z \\ Q \end{bmatrix},$$

$$E_t = \rho\left(\frac{u^2 + v^2 + w^2}{2} + e\right), \qquad (3)$$

$$Q = Q_J - Q_R + f_x u + f_y v + f_z w,$$

and

$$q_x = -\lambda\frac{\partial T}{\partial x}, \quad q_y = -\lambda\frac{\partial T}{\partial y}, \quad q_z = -\lambda\frac{\partial T}{\partial z}, \qquad (4)$$

complemented by the equations of state

$$p = p(\rho, e), \quad T = T(\rho, e), \qquad (5)$$

where ρ, T, and p denote the gas density, temperature, and pressure, respectively; u, v, and w are components of the gas velocity vector $\mathbf{v}$; E_t is the total energy per unit volume of gas; e is the internal energy per unit mass of gas; f_x, f_y, and f_z are components of the vector of force $\mathbf{f}$ acting on the gas along the x, y, and z axes, respectively; Q_J is the volumetric power of Joule dissipation, and Q_R is the variation of energy due to radiative heat transfer; and λ is the thermal conductivity coefficient of gas.

The initial conditions for Eqs. (1)–(5) are preassigned in the form of distributions of temperature, pressure, and velocity,

$$T(x, y, z, t)|_{t=0} = T_0(x, y, z),$$

$$p(x, y, z, t)|_{t=0} = p_0(x, y, z),$$

$$u(x, y, z, t)|_{t=0} = u_0(x, y, z),$$

$$v(x, y, z, t)|_{t=0} = 0, \quad w(x, y, z, t)|_{t=0} = 0.$$

The boundary conditions are defined by the parameters of supersonic flow at the channel inlet,

$$T(x, y, z, t)|_{x=0} = T_1(y, z, t),$$

$$p(x, y, z, t)|_{x=0} = p_1(y, z, t),$$

$$u(x, y, z, t)|_{x=0} = u_1(y, z, t),$$

$$v(x, y, z, t)|_{x=0} = 0, \quad w(x, y, z, t)|_{x=0} = 0,$$

and "soft" boundary conditions, i.e., equality to zero of the derivatives of the sought quantities, are preassigned at the outlet,

$$\left.\frac{\partial T(x, y, z, t)}{\partial x}\right|_{x=L} = 0, \quad \left.\frac{\partial p(x, y, z, t)}{\partial x}\right|_{x=L} = 0,$$

$$\left.\frac{\partial \mathbf{v}(x, y, z, t)}{\partial x}\right|_{x=L} = 0.$$

Impermiability conditions preassigned on the side walls of the channel.

The following equations are solved in order to calculate the volumetric variation of energy Q_R due to radiative transfer:

$$\boldsymbol{\Omega} \cdot \mathrm{grad}(I_\nu) = k_\nu(I_{\nu p} - I_\nu), \qquad (6)$$

$$\mathbf{W} = \int_0^\infty d\nu \int \mathbf{a} I_\nu d\Omega, \qquad (7)$$

$$Q_R = \mathrm{div}(\mathbf{W}), \qquad (8)$$

where I_ν is the intensity of energy of radiation of frequency ν, $I_{\nu p}$ is the intensity of equilibrium radiation, $k_\nu(\nu, T, p)$ is the radiation absorption coefficient, $\mathbf{a}$ is the unit vector which defines the direction of radiation for angle $d\Omega$, and $\mathbf{W}$ is the vector of radiation energy flux.

The boundary conditions for the equation of radiative transfer (6) are defined by the radiation which is incident from without: $I_\nu|_\Gamma = I_{0\nu}(\mathbf{a}, \nu)|_\Gamma$, where Γ is the boundary of the computational domain for radiation, and **a** is the vector which defines the direction of radiation. In these calculations, the channel walls were assumed to be much colder than the radiating gas; therefore, $I_\nu|_\Gamma = 0$.

The electrodynamic part of the problem was formulated in view of the smallness of induced magnetic field B_{ind} whose value was estimated by the formula for an infinite straight conductor,

$$B_{\text{ind}} = \mu_0 I/(2\pi r).$$

Here, $\mu_0 = 4\pi\times10^{-7}$ H/m is the magnetic constant, and r is the conductor radius. We will determine the electric current $I = \varepsilon/R$ flowing in the "current layer–electrodes–load" circuit by the values of electromotive force $\varepsilon = u_T B_0 H$ and of circuit resistance $R = R_{\text{dis}} + R_L = 2R_{\text{dis}}$; in so doing, the load resistance R_L is taken to be equal to the resistance of the discharge region $R_{\text{dis}} = \text{H}/(\pi r^2\sigma)$, which corresponds to the value of load factor $K = 0.5$ (H is the interelectrode spacing). As a result, we derive the expression for the ratio $B_{\text{ind}}/B_0 = \mu_0\sigma u_T r/4 = 0.25\text{Re}_m$ (the presence of numerical coefficient before the magnetic Reynolds number Re_m is associated here with the inclusion of external load and discharge geometry). The value of induced magnetic field is low ($B_{\text{ind}}/B_0 < 0.1$) for the characteristic parameters of the MGD process, namely, the electrical conductivity of gas in the discharge region $\sigma = 3\times10^3$ $\text{Ohm}^{-1}\text{m}^{-1}$, the velocity of the current layer $u_T = 10^3$ m/s, and the radius of the discharge region $r \le 0.1$ m.

A set of Maxwell equations in the approximation of static electrodynamics is used to describe the MGD interaction; in so doing, the permittivity and magnetic permeability of the medium are taken to be unity,

$$\mathbf{j} = \sigma(\mathbf{E}^e + \mathbf{E}^{\text{ext}}), \quad (9)$$

$$\text{rot}\mathbf{E}^e = 0, \quad (10)$$

$$\text{div}\mathbf{E}^e = 4\pi\rho_e, \quad (11)$$

where $\mathbf{E}^e(x, y, z)$ is the electric field intensity defined by external load, $\mathbf{E}^{\text{ext}}(x, y, z) = \mathbf{v}\times\mathbf{B}$ is the induced electric field intensity, $\mathbf{j}(x, y, z)$ is the field of current density, and $\rho_e(x, y, z)$ is the field of density of electric charges.

We use the scalar function of electric field potential $\varphi(x, y, z)$, which satisfies the equation

$$-\nabla\varphi = \mathbf{E}^e, \quad (12)$$

and the relation $\text{div}\mathbf{j} = 0$ to derive an inhomogeneous elliptic equation with variable coefficients,

$$\text{div}(\sigma\nabla\varphi) = \text{div}(\sigma\mathbf{E}^{\text{ext}}). \quad (13)$$

The solution of this equation enables one to find the distribution of potential $\varphi(x, y, z)$, by which the electric field $\mathbf{E}^e$ is determined from Eq. (12) and, with the aid of Eq. (9), the distribution of density of currents **j**. The values of Joule dissipation and of the bulk Lorentz force acting on conducting gas are calculated as follows:

$$Q_J = \mathbf{j}^2/\sigma, \quad \mathbf{f} = \mathbf{j}\times\mathbf{B}. \quad (14)$$

The values of potential are preassigned as the boundary conditions of Eq. (13) on the electrodes; on the nonconducting boundaries, where the normal component of current density is absent, the respective derivative of potential is equated to zero.

Computational Algorithm

The numerical solution of the problem on each time layer is performed in three stages.

1. The distribution of Q_R is determined from Eqs. (6)–(8) by the values of temperature and pressure from the current time layer at each point of the grid.

2. Electrodynamic equations (9)–(14) are used to find the distribution of current density and the electric field intensity, by which the bulk electrodynamic force **f** and Joule dissipation Q_J are calculated at each point of the computational domain.

3. The gasdynamic equations (1)–(5) are solved.

As in [1], a multi-group approximation is used to calculate the radiative transfer. The method of characteristics (S_n-method) is used for numerical solution of Eq. (6) [2, 3]; this method is based on the choice of characteristic directions, with one-dimensional equation of transfer solved along each one of those directions. In a three-dimensional formulation, the directions are preassigned by way of connecting the node being treated with all 26 nearest difference points. Equations of radiative transfer are solved for all directions; the algorithm of solution is described in [1].

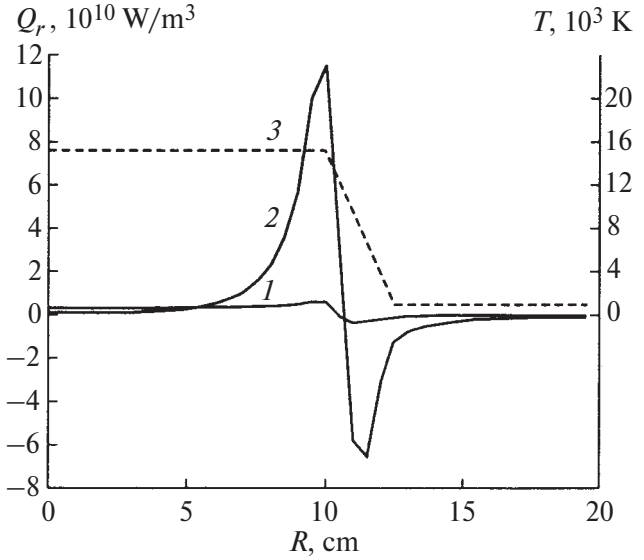

Fig. 2. The distribution of (*1*, *2*) bulk energy loss $Q_R(r)$ and (*3*) temperature in a cylindrical volume of air.

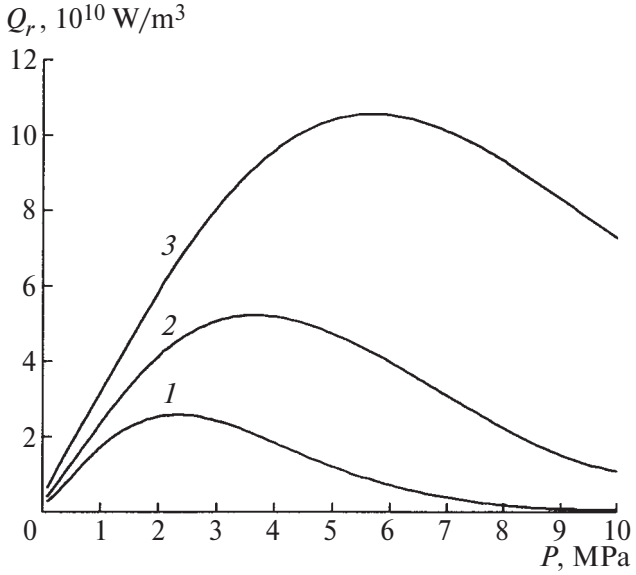

Fig. 3. The pressure dependence of radiative energy loss $Q_R(p)$ at the center of cylindrical volume of air for (*1*) δ = 0.2 m, (*2*) 0.1 m, and (*3*) 0.05 m.

The electrodynamic equation (13) is solved using the time relaxation method, which consists in that the respective unsteady-state equation

$$\frac{\partial \varphi}{\partial t} = \mathrm{div}(\sigma \nabla \varphi) - \mathrm{div}(\sigma \mathbf{E}^{\mathrm{ext}}) \qquad (15)$$

is used to find the solution reduced to the steady state. The numerical solution of Eq. (15) is derived by the economical scheme of splitting over space directions [4] using an implicit difference scheme.

In the third stage, the explicit McCormack scheme with splitting over space coordinates [5] is used to solve Eqs. (1)–(5). This approach makes it possible to reduce the solution of three-dimensional problem to successive solution of a set of one-dimensional gasdynamic problems. In order to determine the unknown quantities on the new time layer, one-dimensional operators are employed, which are used in a symmetrical sequence providing for the second order of approximation with respect to both time and space,

$$\mathbf{U}^{n+2}_{i,j,k} = L_x(\tau)L_y(\tau)L_z(\tau)L_z(\tau)L_y(\tau)L_x(\tau)\mathbf{U}^{n}_{i,j,k}.$$

The one-dimensional difference operator is determined similarly [1].

A more detailed description of numerical algorithm and of the results of calculations of test problems is given in [6].

CALCULATION RESULTS

Characteristics of Radiative Heat Transfer

The efficiency of MGD interaction and the structure of current layer are largely defined by the energy balance, one of whose basic components is radiation. In order to investigate the special features of radiative heat transfer in the current layer, the dependences of radiant energy loss Q_R on pressure and size for the center of cylindrical air region were obtained from the solution of equations of radiative transfer. The same values of the cylinder diameter and height were preassigned, with δ = 0.05, 0.1, and 0.2 m. The temperature in the volume was taken to be uniform and equal to $T = 1.5\times10^4$ K; at the cylinder edges the temperature decreased linearly to $T = 10^3$ K (Fig. 2). The values of the absorption coefficient were preassigned in the form of tables $k_\nu(\nu, T, p)$ [7]. In so doing, 560 frequency intervals were used in the range from 2.5×10^2 cm^{-1} to 1.4×10^5 cm^{-1}.

The $Q_R(p)$ dependences for all values of δ have a maximum (Fig. 3). The value of the maximum and that of the corresponding pressure decrease with increasing δ. The initial linear segment of the rising branch of $Q_R(p)$ dependences corresponds to the volume pattern of radiation, when the optical thickness of the region is small for most of the spectrum,

$l_\nu = k_\nu\delta << 1$. In this case, the medium is optically transparent, and the radiation leaves all zones of the volume without marked absorption. At pressures $p \approx$ $\approx$ 0.1 MPa, about 50% of power is radiated in the lines. The absorption coefficient increases almost directly with pressure; therefore, the relation $l_\nu >> 1$ is valid for the majority of frequencies starting with some value of p, and the absorption becomes a factor which inhibits the departure of radiation from the volume and affects significantly the pattern of energy loss in gas. Corresponding to this pressure range is the descending branch of the $Q_R(p)$ curve; in so doing, the bulk of energy released in the central region does not leave the volume freely but is absorbed by the neighboring regions of gas. In this mode, the energy is largely carried away in the continuous spectrum and from the edges of the volume; therefore, the radiation exhibits largely a surface pattern. Figure 2 gives the $Q_R(r)$ distributions for pressure values of 0.1 and 10 MPa. In the case of high pressure, the maximum of $Q_R(r)$ is located at the edge of the radiating volume, and its value is more than an order higher than the value of Q_R at the center. In the case of low pressure, the radiation is volumetric, and the distribution of Q_R is much more uniform. In the region of temperature decrease, the gas absorbs vigorously the radiation energy, and this mechanism provides for the possibility of increasing the size of the discharge region.

Most promising for the MGD process from the standpoint of minimizing the loss of energy from the current layer are modes with volume radiation at low pressure ($p < 1$ MPa) and with surface radiation at fairly high values of pressure ($p > 5$ MPa) and size of the current layer ($\delta \geq 0.2$ m). We will consider the characteristic features of formation of current layer in these modes in a supersonic air flow described using the ideal gas model with the adiabatic exponent $\gamma = 1.3$ and molar mass $\mu = 28.9$ g/mol. The coefficients of electrical conductivity and thermal conductivity were preassigned in the form of tables $\sigma(T, p)$ and $\lambda(T, p)$ [8].

The Structure of Current Layer at Low Pressure

The dynamics of flow at low pressure were simulated for a channel of length $L = 0.5$ m, width $W =$ $= 0.1$ m, and height $H = 0.1$ m with the following process parameters: the induction of external magnetic field $B = 2$ T, the load resistance $R_L = 2\times10^{-3}$ Ohm, and the velocity, temperature, and pressure at the channel inlet $u = 2$ km/s, $T = 10^3$ K, and $p = 0.1$ MPa, respectively. In the initial state, a gasdynamic flow includes a discharge region preassigned in the form of a regular cylinder of radius $r = 0.05$ m and temperature $T = 10^4$ K. The number of grid nodes in this calculation was 101×21×21.

The interaction with magnetic field causes stagnation of the current layer and formation of flow mode. The incident flow breaks the external layer of hot gas away from the edges of the discharge region; in so doing, a vortex flow is formed downstream, whose structure reminds of the Karman street. Figure 4a gives the instant of time which precedes the next separation of two conducting filaments from the discharge edges; in what follows, they are carried away downstream, cool down gradually, and cease interacting with the magnetic field. In the initial stage ($t <$ < 0.2 ms), the discharge region retains the symmetric shape, and the gas flow is two-dimensional. With time the discharge symmetry is lost, and its size and shape begin to vary randomly in the neighborhood of some average values (Fig. 4b). This behavior of discharge region is due to several reasons. The periodic separation of vortexes from the discharge edges leads to the emergence of a transverse force which causes a fluctuating variation of the discharge shape. Another reason is the possible development of Rayleigh–Taylor instability, when tongues of cold gas penetrate into the conducting region, this leading to the division of discharge or to separation of parts of different sizes from this discharge. One can see in Fig. 4c the initial stage of RTI at the discharge center; this stage develops in the form of a local bubble rather than over the entire height of conducting channel. The development of this RTI resulted in the separation of a fairly large part of discharge, which caused a strong variation of its spatial shape. After a time, the separated region cooled down, and the discharge recovered its characteristic shape and size (Fig. 4d).

The results of this numerical experiment demonstrate the basic features typical of the dynamics of current layer at low pressure, namely, the formation of flow past the discharge region and possible (but not mandatory) development of RTI. The variation of the parameters of the initial discharge region and of other initial parameters of the process may bring about a diversity of configurations of current layer and significant changes in the dynamics of MGD interaction.

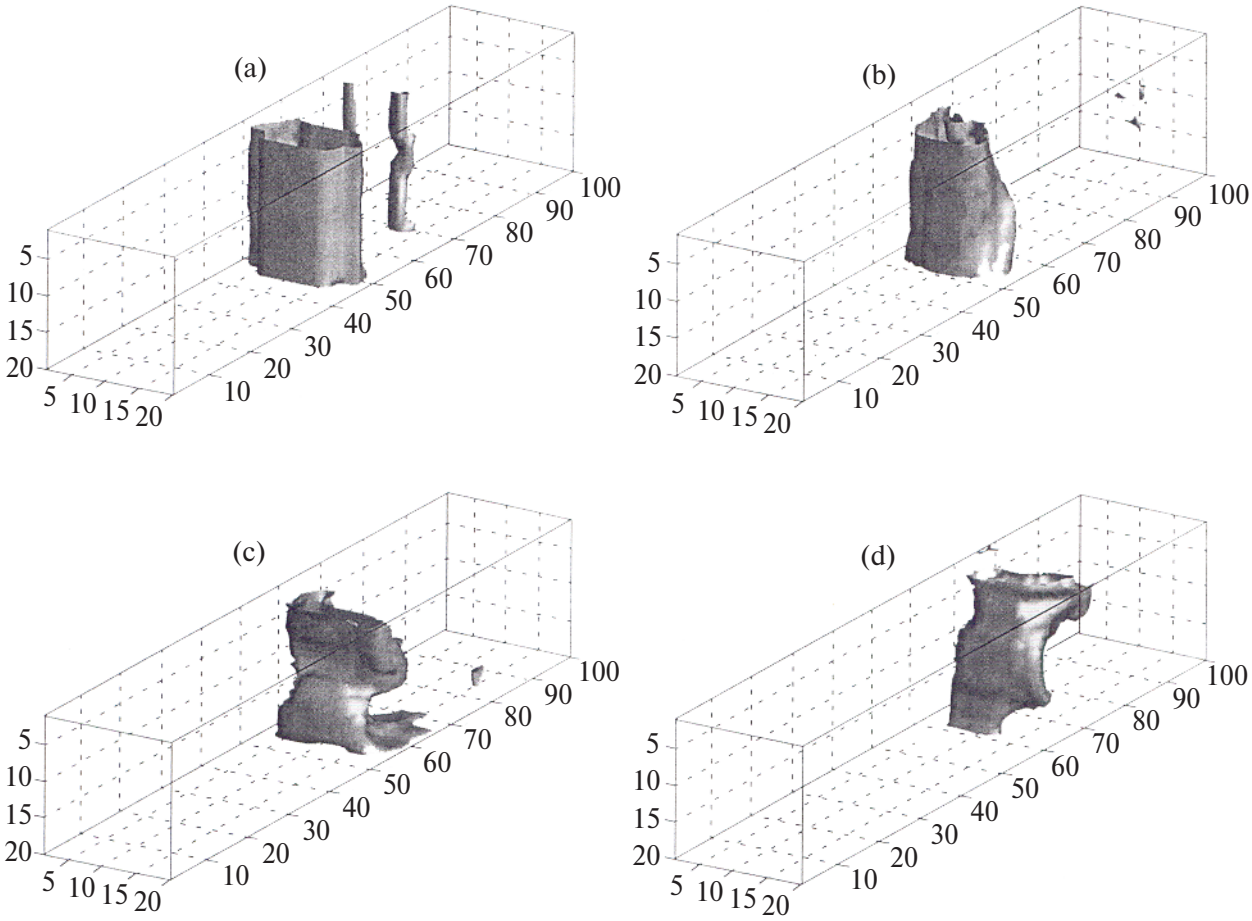

Fig. 4. Surfaces at constant temperature (T = 9000 K), which correspond to different instants of time: (a) 0.2 ms, (b) 0.4 ms, (c) 1, (d) 1.2 ms (given on the axes are the numbers of calculation points).

The Structure of Current Layer at High Pressure

We will consider the process of MGD interaction at high pressure with the following parameters: the induction of external magnetic field B = 6 T; the load resistance $R_L = 10^{-3}$ Ohm; the velocity, temperature, and pressure at the channel inlet u = 2 km/s, T = = 1000 K, and p = 6 MPa, respectively; the radius of the initial discharge region r = 0.1 m, and the temperature in this region $T = 10^4$ K. The calculation was performed for a channel of L = 1 m, W = 0.2 m, and H = 0.1 m, with the number of grid nodes of 201×41×41.

The interaction with magnetic field causes stagnation of the current layer and formation of flow mode. In so doing, several RTIs develop symmetrically on the upstream boundary of the discharge and shift to the side boundaries of the discharge under the effect of incident flow (Fig. 5a). With time the instabilities deepen so that their development leads to separation of conducting gas regions of different sizes from the main discharge (Fig. 5b). The smallest of these regions are carried away by the flow to the expansion wave region and, because of the higher level of radiative energy loss, they cool down gradually and cease interaction with the magnetic field. The largest region, which is likewise located downstream, approaches the main discharge owing to return vortex flows, cools down partly and decreases in size, and is then combined with the main discharge (Fig. 5c). At the same instant of time, the development of RTI at the discharge center is observed, where a jet is formed which divides the discharge in the middle (Fig. 5d). In so doing, the jet does not pass through the entire thickness of the discharge because, upon interaction with counter return flow of gas, it is divided in two jets the directions of whose propagation deviate from the channel axis. In addition, other RTIs develop within the current layer; this results in the formation of a highly nonuniform laminar structure of current layer which almost fully overlaps the channel in mid-section (Fig. 5e). The division of discharge into separate,

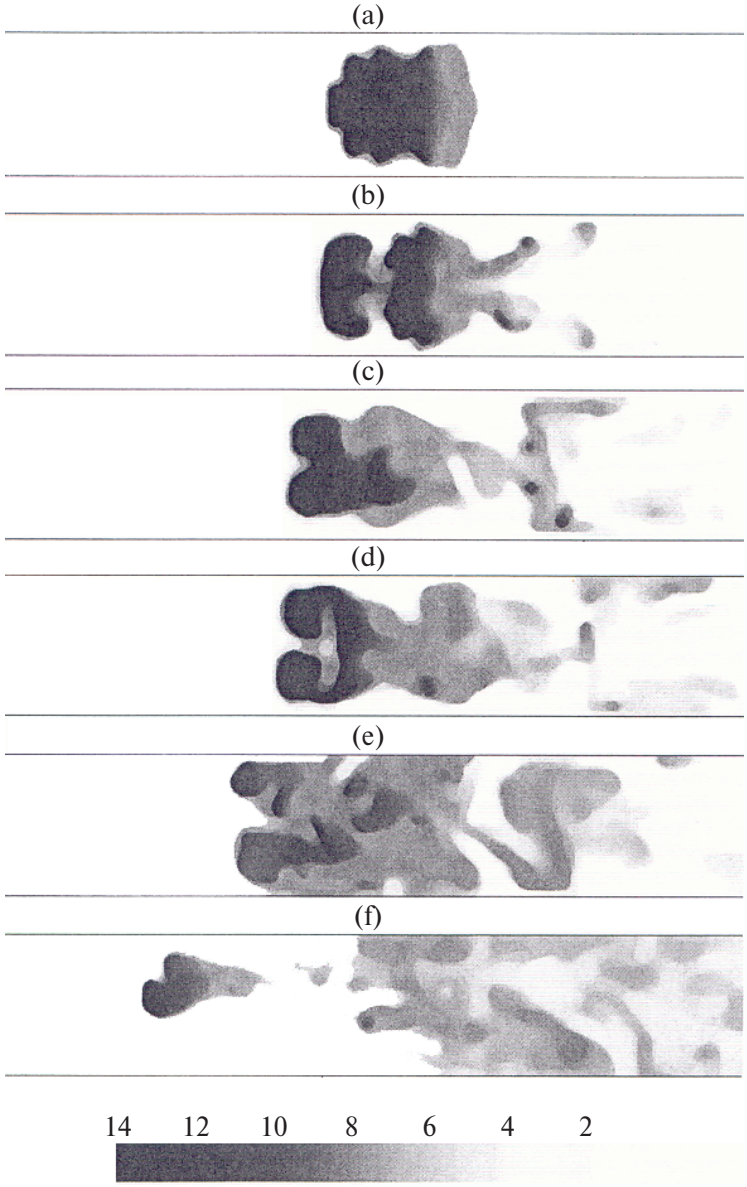

Fig. 5. The distribution of temperature in a plane equidistant from the surface of electrodes for several instants of time: (a) 0.1 ms, (b) 0.3 ms, (c) 0.5 ms, (d) 0.7 ms, (e) 1 ms, (f) 1.4 ms. The temperature scale below is in kK.

relatively thin current-conducting channels leads to intensive convective carryover of energy and increase in the level of radiative energy loss due to the decrease in optical thickness. In so doing, the power of Joule dissipation is no longer sufficient for maintaining a high temperature in the entire volume of the discharge; as a result, all of the discharge regions, with one exception, cool down, cease interacting with magnetic field, and are carried by the flow downstream. The remaining discharge has a transverse dimension of less than 10 cm and, because of the small cross section, interacts with the gas flow relatively weakly (Fig. 5f).

Until the instant of time $t \approx 0.3$ ms, the flow and structure of discharge retained their two-dimensional pattern. A special feature of the process at high pressure is the surface pattern of radiative energy loss which has a maximal value in the "corner" points of discharge that are most removed from the center. The gas cools down here, and this leads to an increase in the current density in the discharge section at the electrode and, in the end, to thermal contraction of the discharge which is expressed in terms of decreasing diameter of the current-conducting channel in the vicinity of the electrodes. Because the deceleration of gas by a bulk electrodynamic force is stronger in the

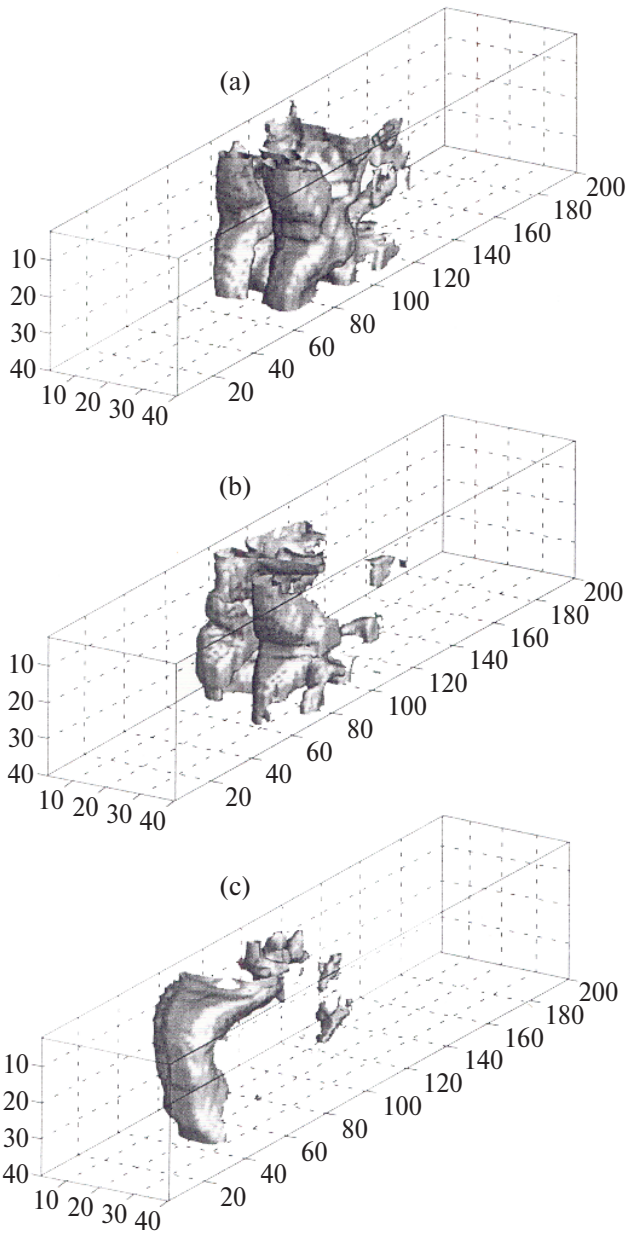

Fig. 6. Surfaces at constant temperature (T = = 9000 K), which correspond to the instants of time (a) 0.5 ms, (b) 1 ms, (c) 1.4 ms.

region of higher density of current, the discharge channels bend (Figs. 6a and 6b). Later on, when only one relatively thin current-conducting channel remains in the channel, the effect of radiation blocking shows up to a smaller degree, and the discharge assumes a more rectilinear shape (Fig. 6c).

Note that the possibility of studying modes with surface radiation at higher pressures was limited by the fact that the data on thermal and radiation properties of air in [7, 8] are given only to pressures of 10 MPa.

Energy Characteristics of the Process

The strength of current and the degree of conversion of enthalpy of flow are some of the main integral characteristics of the process of MGD interaction. Figure 7 gives the time dependences of current which correspond to the investigated processes at low and high pressures. The common feature of these dependences is the initial current rise due to the heating of gas and increasing MGD interaction. After that (t > > 0.3–0.4 ms), the flow past the discharge region is formed, which brings about a decrease in the efficiency of interaction and value of current. The maximal value of current for a process with low pressure is $I_L \approx 20$ kA; in the case of flow past the discharge region, this value decreases to $I_L \approx 6$ kA. By the instant of time $t \approx 1$ ms, RTI in the form of inflating bubble starts developing (Fig. 4c), which results in an increased transverse dimension of the discharge, higher efficiency of the discharge/flow interaction, and rising electric current. After the combined effect of RTI and incident flow caused the separation of a significant region of hot gas from the current layer, the strength of current decreased once again and became steady at $I_L \approx 8$ kA. At high pressure, the maximal value of current strength could be as high as $I_H \approx$ $\approx 6\times10^5$ A, which is defined by the large size of the current layer and by the high value of electrical conductivity of gas. Then, the breakthrough of RTI at the center of the discharge region (Fig. 5d) leads to the current drop to $I_H \approx 1.4\times10^5$ A; after that, the formation of laminar structure of current layer, which almost fully overlaps the channel (Fig. 5e), causes an increase in current to $I_H \approx 2\times10^5$ A for some period of time. The minimal value of current strength ($I_H \approx$ $\approx 1.3\times10^5$ A) corresponds to the period when only one relatively thin current-conducting channel remained in the channel ($t \approx 1.4$ ms). The fluctuation component of the dependences is defined by the variation of shape and size of the current layer during the separation of vortexes.

The most important characteristic of generating process is the degree of conversion of enthalpy of flow which was calculated by the formula

$$\eta_N = \frac{I^2 R_L}{\rho_1 u_1 F(c_p T_1 + u_1^2/2)}.$$

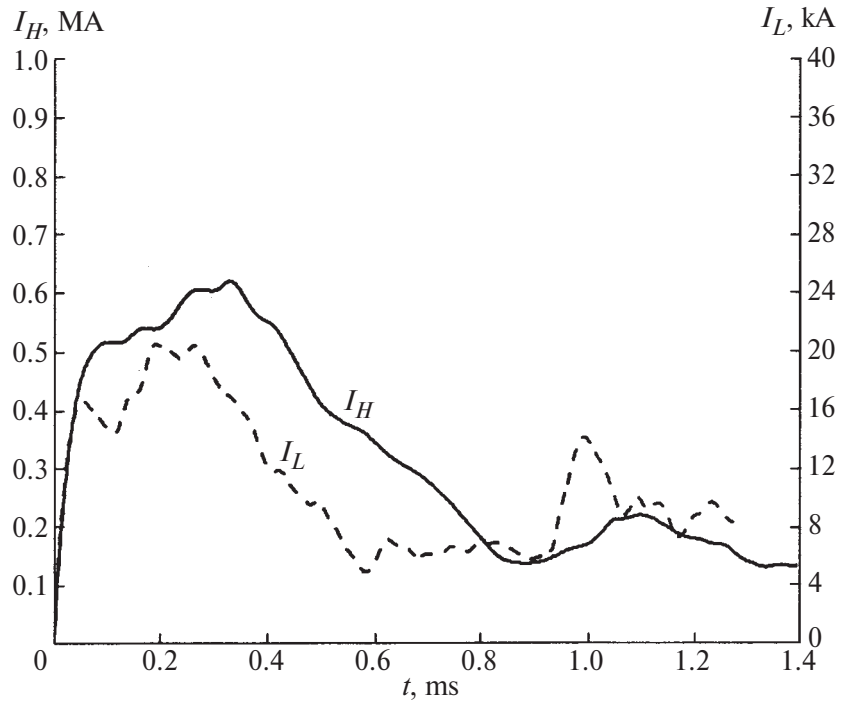

Fig. 7. The time dependence of discharge current I_L, low-pressure mode; I_H, high-pressure mode).

Here, F is the channel cross section, and the values of variables with subscript 1 correspond to the parameters of supersonic flow at the channel inlet. In the low-pressure mode, $\eta_N \approx 3.5\%$ at a current of 20 kA, and the minimal value is $\eta_N \approx 0.4\%$ at a current of 6 kA. In the high-pressure mode, $\eta_N \approx 6.6\%$ at a current of 6×10^5 A, and the minimal value is $\eta_N \approx 0.2\%$ at a current of 1.3×10^5 A.

The integral characteristics of MGD interaction depend significantly both on the spatial structure of the current layer and on other parameters of the MGD process. For example, in the low-pressure mode with varying load resistance, the maximal value of $\eta_N \approx 7\%$ was obtained for $R_L = 4\times10^{-3}$ Ohm. Higher values of η_N may be attained by optimizing the conditions of interaction, because the degree of enthalpy conversion η_N is characterized by complex functional dependences with clearly defined maxima on a whole complex of process parameters [9]. This is a fairly complex problem which calls for separate study.

CONCLUSIONS

The calculations have revealed that the current layer has a complex spatial structure, the formation of which is affected both by the processes of force interaction, which lead to the flow past the discharge region and to the development of Rayleigh–Taylor instability, and by radiative-convective heat transfer which defines the size of discharge, the level of temperature, and the electrical conductivity. The presence of a unified discharge which overlaps the channel cross section provides for the maximal efficiency of MGD interaction, and the division of the current layer into separate relatively thin current-conducting channels leads to an increase in the level of radiative-convective energy loss and to a decrease in the efficiency of interaction of the discharge region with the gas flow and magnetic field.

The suggested model involved the description of external circuit based on preassignment of resistance rather than of load parameter, as was the case in [1]. In this case, the current layer is characterized by a higher energy stability because of redistribution of energy being generated. For example, in the case of reduction of temperature and electrical conductivity of gas, the increase in ohmic resistance of the discharge region causes an increase in $R_{\text{dis}}/(R_{\text{dis}} + R_L)$ and in the fraction of Joule dissipation in the overall energy balance; in the end, this prevents further cooling of gas. In the reverse process, the power of heat release in the current layer decreases.

REFERENCES

1. Vasil'ev, E.N. and Nesterov, D.A., *Teplofiz. Vys. Temp.*, 2005, vol. 43, no. 3, p. 401 (*High Temp.* (Engl. transl.), vol. 43, no. 3, p. 396).
2. Chetverushkin, B.N., *Matematicheskoe modelirovanie zadach dinamiki izluchayushchego gaza* (Mathematical Simulation of Problems in Dynamics of Radiating Gas), Moscow: Nauka, 1985.
3. Adrianov, V.N., *Izv. Akad. Nauk SSSR*, 1988, no. 2, p. 142.
4. Samarskii, A.A., *Teoriya raznostnykh skhem* (The Theory of Difference Schemes), Moscow: Nauka, 1989.
5. Anderson, J., Tannehill, J., and Pletcher, R., *Computational Hydrodynamics and Heat Transfer*,, New York: Hemisphere, 1984. Translated under the title *Vychislitel'naya gidrodinamika i teploobmen*, Moscow: Mir, 1990, vol. 2.
6. Vasil'ev, E.N. and Nesterov, D.A., *Vychisl. Tekhnol.*, 2005, vol. 10, no. 6, p. 13.
7. Avilova, I.V, Biberman, L.M., Vorob'ev, V.S. *et al.*, *Opticheskie svoistva goryachego vozdukha* (Optical Properties of Hot Air), Moscow: Nauka, 1970.
8. Sokolova, I.A., *Zh. Prikl. Mekh. Tekh. Fiz.*, 1973, no. 2, p. 80.
9. Vasil'ev, E.N., Derevyanko, V.A., and Slavin, V.S., *Teplofiz. Vys. Temp.*, 1986, vol. 24, no. 5, p. 844.